PyTOAST: Python Top Of Atmosphere Simulation Tool

Amir Ibrahim, Sean Bailey, Bryan Franz, and Jeremy Werdell

Document version 1.0: 23 April 2021

Introduction

PyTOAST generates simulated top-of-atmosphere Level-1B files for the PACE Ocean Color Instrument (OCI). PyTOAST utilizes retrieved surface and atmospheric properties and top-of-atmosphere (TOA) radiances from MODIS and VIIRS, pre-computed radiative-transfer look-up tables for the OCI spectral response, and spectral libraries of land and clouds to produce realistic radiometry in the standard Level-1B format (https://oceancolor.gsfc.nasa.gov/data/pace/format/) of OCI. The PyTOAST simulator is computationally efficient, and thus allows for large scale production of multi-day global data distributions with realistic viewing geometries for testing retrieval software mechanics and data flow.

Theoretical Background

Clear sky ocean model

The simulator is based on a radiative coupling of various components of the atmosphere, ocean, and land surfaces as an inverse process to the atmospheric correction (Mobley et al., 2016). For a clear ocean pixel, the top-of-atmosphere (TOA) reflectance is calculated as follows:

$$\rho_t(\lambda; Geom) = \left(\rho_{path}(\lambda; Geom) + \rho'_w(\lambda; Geom) + \rho'_{surface}(\lambda; Geom)\right) \times T_g(\lambda; Geom). \quad (1)$$

The TOA reflectance is a function of $Geom$ (i.e. solar zenith; θ_0, sensor zenith θ, and relative azimuth φ), and wavelength, λ; $\rho_{path}(\lambda; Geom)$ is the path reflectance due to scattering and absorption by air molecules (Rayleigh scattering) and aerosols; $\rho'_w(\lambda; Geom)$ is the ocean body reflectance, and $\rho'_{surface}(\lambda; Geom)$ is the reflectance contribution from surface glint and whitecaps, where both $\rho'_w(\lambda; Geom)$ and $\rho'_{surface}(\lambda; Geom)$ are expressed at the TOA after propagation through the atmosphere. $T_g(\lambda; Geom)$ is the two-way absorbing gas transmittance along the solar and sensor zenith. In the following sections we will briefly discuss each of the above terms.

Path reflectance:

The path reflectance is a summation of two terms, the Rayleigh reflectance and the aerosol reflectance including the aerosol-Rayleigh interaction:

$$\rho_{path}(\lambda; Geom) = \rho_r(\lambda; Geom) + \rho_a(\lambda; Geom). \quad (2)$$

Draft

The $\rho_r(\lambda; Geom)$ term is calculated through the tabulation of vector radiative transfer (VRT) simulations. The Rayleigh optical depth, which is input to the VRT code, is calculated from Bodhaine et al. (1999). Although the path reflectance term is shown in Eqs. (1) and (2) as a function of only wavelengths and geometry, the Rayleigh reflectance is also a function of atmospheric surface pressure and surface windspeed, where the surface roughness model is based on the Cox-Munk windspeed to wave slopes relationship and the effect of pressure variation is modeled from Wang (1995).

The second term in Eq. (2) is the aerosol reflectance, which is calculated through the VRT code for 80 different aerosol models from Ahmad et al. (2010), where the microphysical properties of the aerosol models are calculated for a pre-determined set of 8 near-surface atmospheric relative humidities and 10 fine-mode volume fractions, and the aerosol vertical profile in the atmosphere is based on the Shettle and Fenn model (Shettle and Fenn 1979). The aerosol reflectance calculations include effects of multiple scattering and molecule-aerosol interaction within the atmosphere. The molecule-aerosol diffuse transmittance along the solar and sensor directions, $t_{sol}(\lambda, Geom)$ and $t_{sen}(\lambda, Geom)$, respectively, is also calculated and tabulated from the VRT simulations, and used to propagate the water and surface reflectance to the TOA.

Ocean reflectance:

$\rho'_w(\lambda; Geom)$ is the ocean reflectance at TOA. The bottom of atmosphere (BOA) ocean reflectance $\rho_w(\lambda; Geom)$ is calculated through a forward model that provides the ocean reflectance as a function of chlorophyll-a (Chl-a; mg m^{-3}) concentration and $Geom$. The BOA reflectance contribution is attenuated by the diffuse transmittance of the atmosphere, such that $\rho'_w(\lambda; Geom) = t_{sen}(\lambda, Geom) \times \rho_w(\lambda; Geom)$. The BOA ocean reflectance is based on the Morel and Maritorena (2001) ocean reflectance model (ORM) for open ocean waters as modified in Werdell et al. (2007), where the only driver of optical variability is phytoplankton abundance as described by Chl-a. The ORM generates a reliable surface reflectance $R_{rs}(\lambda; sr^{-1})$ for the full visible spectrum (Werdell et al., 2007), however it does not account for inelastic scattering, chlorophyll fluorescence, or more complex water types (e.g., sediments, riverine discharge). Following Werdell et al. (2007), the modeled $R_{rs}(\lambda)$ is converted from nadir geometry to the desired solar and sensor path geometry using the bidirectional reflectance distribution function (f_{brdf}) of Morel et al. 2002, and then propagated to the TOA as:

$$\rho'_w(\lambda; Geom) = \pi R_{rs} t_{sol} t_{sen} / f_{brdf}. \quad (3)$$

Ocean surface reflectance:

The surface reflectance, $\rho'_{surface}(\lambda; Geom)$, is the light scattered by the air-sea interface. It has two terms: the direct sun glint reflectance and the whitecap reflectance, both of which are driven by the ocean surface windspeed. It's important to remember that the sky glint reflection was calculated through the VRT model of the Rayleigh signal. The direct glint signal, however, is calculated by the two-way attenuation of the direct solar beam that is modulated by the surface glint reflectance, $L_{GN}(\lambda)$, which is modeled using Cox and Munk (1954) wave slope statistics. The TOA direct glint reflectance is then $\pi L_{GN} T_{sol} T_{sen} / \mu_0$, where μ_0 is the cosine of the solar zenith angle, and spectral (and geometric for *T*) dependency is implied.

Draft

The whitecap irradiance reflectance at the BOA, $\rho_{wc}(\lambda)$, is based on Koepke (1984) combined with the windspeed-dependent fractional coverage model of Stramksa and Petelski (2003) and the whitecap albedo spectral-dependence in the red and near-infrared from Frouin et al. (1996). The BOA irradiance reflectance is then propagated to TOA similar to the ocean reflectance as $\rho_{wc}t_{sol}t_{sen}$, with spectral and geometric dependency implied.

Absorbing gas transmittance:

The PyTOAST simulator accounts for the main absorbing gases in the atmosphere, including ozone, water vapor, and oxygen. The water vapor and oxygen transmittance are based on the HITRAN 2012 line by line (LBL) spectroscopic dataset (Rothman et al. 2013). We calculate the LBL transmittance for different column water vapor (cwv) values assuming the US standard atmospheric profile. Then we apply the instrument spectral response function to the LBL transmittances and we store them in a LUT. The spectral water vapor transmittance at each $Geom$, T_{wv}, is then interpolated from the LUT for a given slanted water vapor (wv) concentration along the path as cwv/μ, where μ is the cosine of the path zenith angle. The oxygen transmittance is calculated similarly for different path lengths of the atmosphere given the observations geometry. The ozone transmittance is calculated from the ozone optical depth assuming Beer's law, where the optical depth is determined from the spectral ozone absorption coefficient and the ozone concentration. The ozone absorption coefficients are tabulated from Anderson (1993), and spectrally integrated with the sensor spectral response functions.

Clear sky land model

Similar to propagating the ocean surface reflectance to TOA, the land reflectance at the bottom of the atmosphere is propagated to TOA by accounting for the diffuse transmittance of the aerosols and air molecules as follows:

$$\rho'_{surface}(\lambda; Geom) = \rho_{land}(\lambda; Geom)t_{sol}(\lambda; Geom)t_{sen}(\lambda; Geom)$$

ρ_{land} is the land reflectance model which uses a slope parameter derived from an OMI/Aura 0.5 degree resolution surface reflectance file (DOI:10.5067/Aura/OMI/DATA3006). This static file contains a spectral slope parameter derived from the 418nm and 499nm bands. This slope parameter is used as a weighting function for two hyperpsectral land reflectances, one soil and one grass. These spectra were obtained from the ECOSTRESS spectral library (https://speclib.jpl.nasa.gov/) for the wavelengths range of 400nm to 2496nm. The UV land reflectance for OCI is extrapolated.

Draft

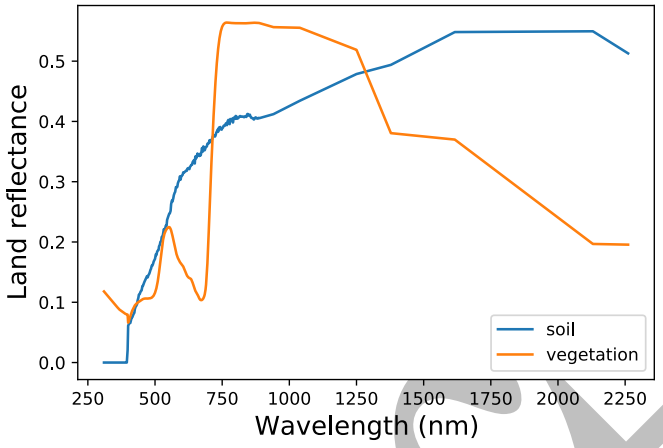

Figure 1: Land reflectance for soil and vegetation from the ECOSTRESS spectral library.

The cloudy sky model

Clouds are estimated using a VIIRS L3 mapped file (global 2km dailies) that includes cloud albedo and TOA radiance at 551nm. The albedo is used to identify where clouds exist and the Lt_551 product is used to scale a predefined hyper-spectral cloud radiance field of liquid cloud simulated using LibRadtran package. The simulation was done with the cdisort solver (4 streams, plane parallel) and Kurudz solar spectrum together with moderate-resolution REPTRAN trace gas absorption parametrization for the US standard atmosphere for Rayleigh and gas (no aerosols). The surface is Lambertian with an albedo of 0.1 (at all wavelengths). The cloud has an optical thickness of 6 (at 550 nm). The effective radius is 10 microns, in a homogeneous layer between 1.5 and 2 km. The solar zenith angle is 30 degrees, relative azimuth 35, and cosine of view azimuth is 0.8.

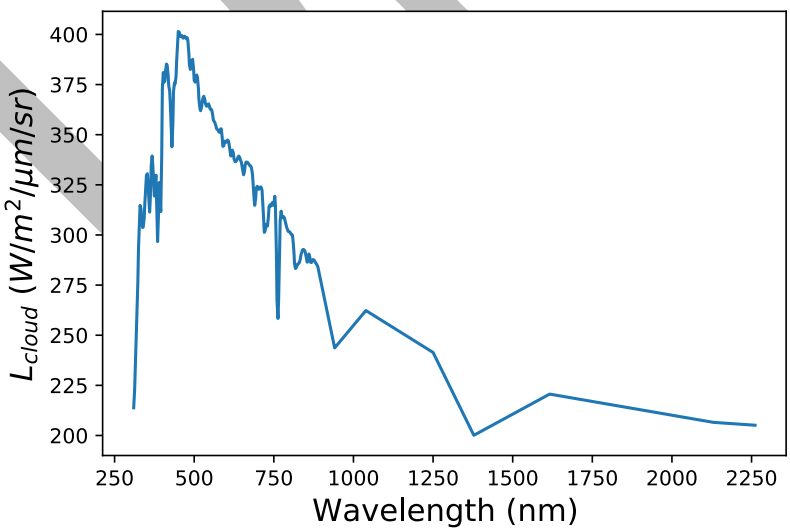

Figure 2: A simulated cloud radiance at TOA using LibRadtran for liquid cloud with optical depth of 6 at 550nm.

Draft

Implementation

PyTOAST flow diagram

PyTOAST relies on modeling the TOA observations based on realistic geophysical data retrieved from ocean color sensors as well as global models such as MERRA-2. The figure below shows the flow diagram of data, where the orbit geometries from OCI, metrological data from MERRA-2, and Level-3 geophysical data from MODIS, VIIRS, and OMI are used as an input to the pre-computed RT forward model LUT.

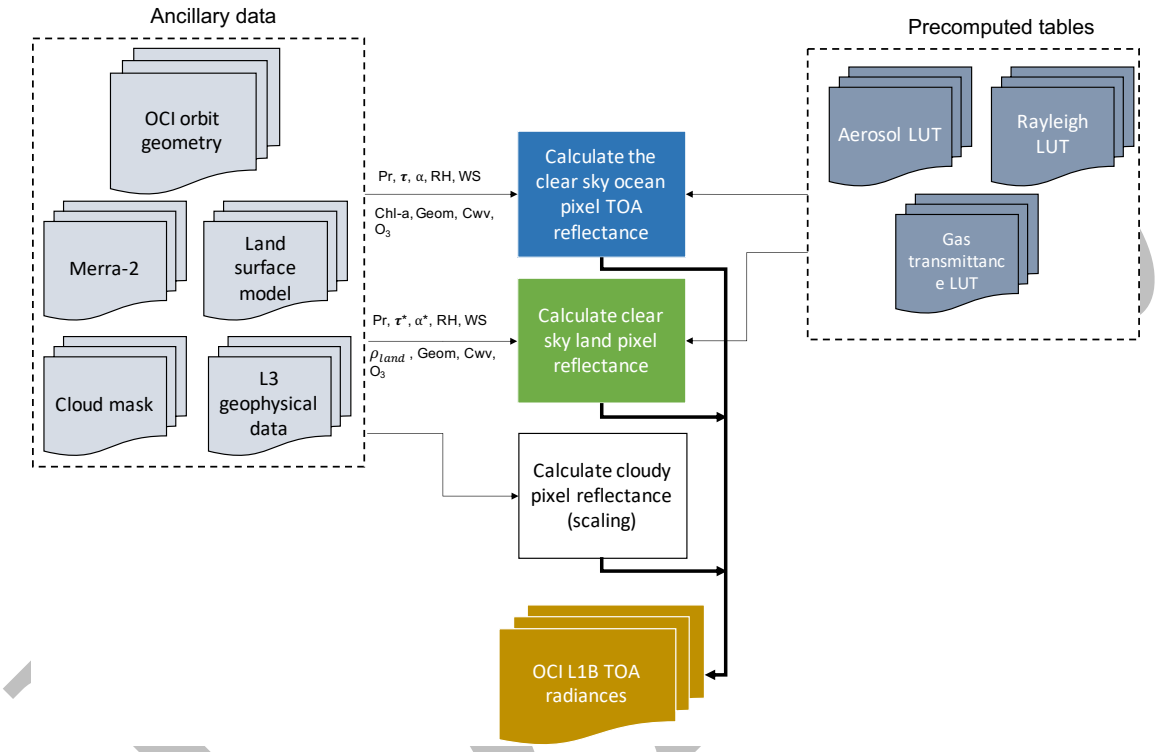

Figure 1: Flow diagram of PyTOAST

A multidimensional interpolation process of the pre-computed LUT calculates the aerosol and molecular scattering, the gas absorption of the atmosphere, and the surface radiance of land and ocean, as well as the cloud reflectances. The TOA radiance is then calculated by multiplying the reflectance with $\mu_0 F_0 f_{sol}$, where F_0 is the solar irradiance (Thuillier et al 2003), f_{sol} is the earth-sun distance correction factor, and spectral dependence is implied. The output TOA radiance is then stored in a standard Level 1B format NetCDF file.

Figure 2 shows an illustration of the TOA radiance, $L_t(\lambda)$, calculation for clear sky ocean pixels without clouds. The aerosol optical depth is coming from the GMAO aerosol transport model, MERRA-2, at ~50 km spatial resolution. The aerosol type used is proportional to the aerosol angstrom coefficient. The aerosol radiance is also calculated from MODIS Aqua Level-3 32-day rolling average Angstrom coefficients at 4 km spatial resolution, while the relative humidity,

needed for the aerosol modeling is taken from meteorological data from MERRA-2 at ~50 km resolution. Wind speed, ozone concentration, water vapor, and surface pressure are also coming from MERRA-2 at 50 km. The ORM model calculates the $R_{rs}(\lambda)$ given the Chl-a concentration from the Level-3 32-day rolling average from MODISA. Finally, the earth-sun distance is calculated for each pixel to adjust the TOA radiance level.

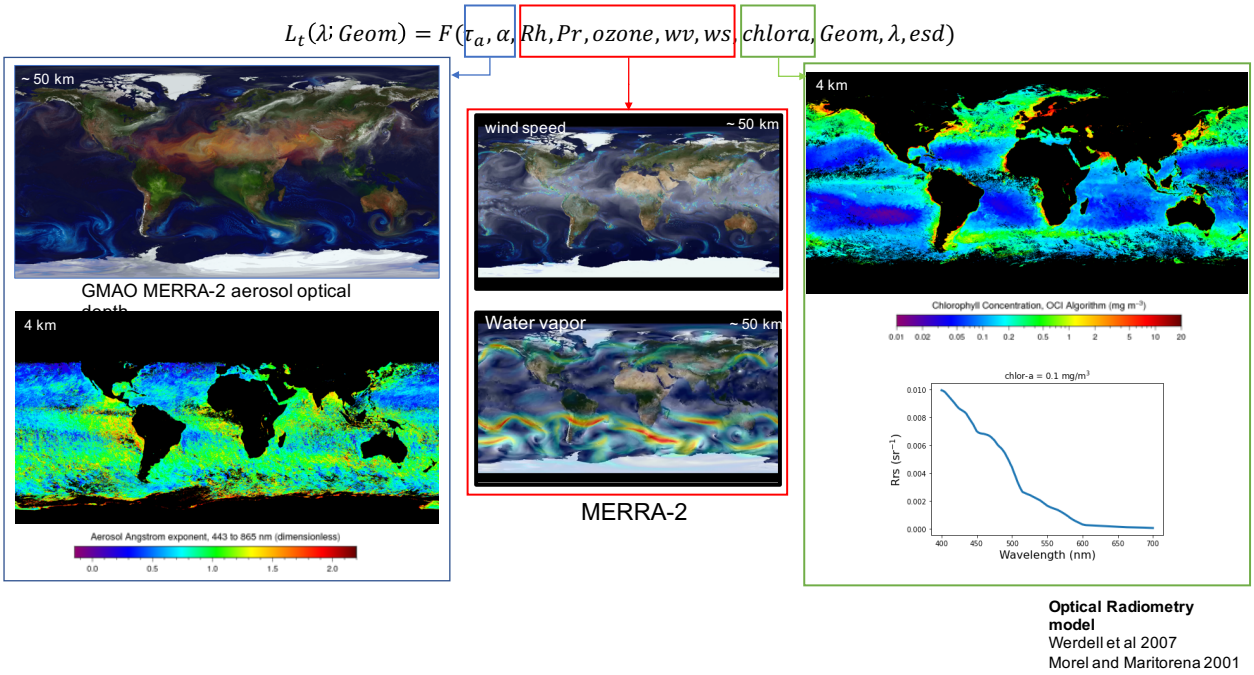

Figure 2: Illustration of the TOA radiance calculation for clear sky ocean pixel.

For clear sky land pixels, we simply rely on an OMI/Aura-derived land reflectance file at 0.5 degree resolution, where each file contains a spectral slope parameter derived from the 418 nm and 499 nm bands. That slope is used as a weighting function for two hyperspectral land reflectances, one soil and one grass.

Dr

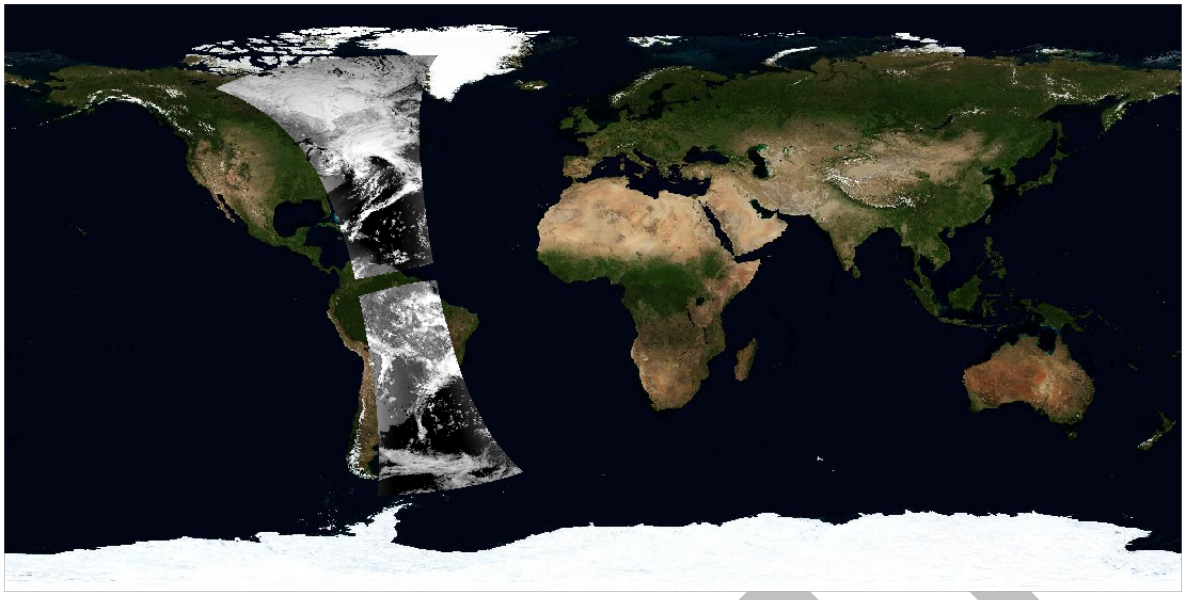

Figure 3: An orbit example demonstrating the PyTOAST simulations of the TOA radiance as observed from OCI for March, 22nd , 2019.

Cloudy pixels are located based on the VIIRS Level-3 cloud mask, where the hyperspectral TOA cloud radiance is scaled given the observed VIIRS TOA radiance at the mid-visible wavelengths.

Figure 3, shows an example of the simulated TOA radiance from PyTOAST for an OCI orbit for March 22nd 2019. The example shows the binned data for various 5-min OCI granules observed along the orbit. The simulation captures a large dynamic range of TOA radiances from ocean, land, and cloudy pixels. The gap along the tropical region is due to the tilting operation of the OCI instrument, as designed to minimize direct sun glint.

Current limitations of PyTOAST

1. The cloud radiance is based on a single liquid cloud radiance spectrum scaled to VIIRS observations.
2. The aerosol models are limited to those of Ahmad et al. (2010), as developed for ocean color atmospheric correction.
3. The ORM bio-optical model only considers Chl-a and constituents that vary with Chl-a (i.e., doesn't account for non-covarying CDOM and minerals typical of coastal waters).
4. The ORM model extrapolates the spectral information beyond the VIS spectrum (i.e. in the UV and SWIR).
5. The UV ozone absorption is not included in the simulations.
6. PyTOAST doesn't fully couple the sub-surface ocean radiance (and land) with the atmosphere.

Table 1: List of Acronyms

Draft

Acronym	Definition
PyTOAST	Python Top of Atmosphere Simulation Tool
PACE	Plankton, Aerosol, Cloud, ocean Ecosystem
TOA	Top of Atmosphere
MODIS	Moderate Resolution Imaging Spectroradiometer
VIIRS	Visible Infrared Imaging Radiometer Suite
OCI	Ocean Color Instrument
LUT	Look up table
VRT	Vector Radiative Transfer
BOA	Bottom of Atmosphere
LBL	Line by Line
cwv	Column water vapor
OMI	Ozone Monitoring Instrument
UV	Ultraviolet
ECOSTRESS	ECOsystem Spaceborne Thermal Radiometer Experiment on Space Station
LibRadtran	Library for radiative transfer
cdisort	C version of Discrete Ordinates Radiative Transfer Program
REPTRAN	Gas absorption parameterization library
GMAO	Global Modeling and Assimilation Office
MERRA-2	Modern-Era Retrospective Analysis for Research and Applications, Version 2
NetCDF	Network Common Data Form
ORM	Optical Radiometry Model
VIS	Visible spectrum

References:

Ahmad, Z., Franz, B.A., McClain, C.R., Kwiatkowska, E.J., Werdell, J., Shettle, E.P. and Holben, B.N., 2010. New aerosol models for the retrieval of aerosol optical thickness and normalized water-leaving radiances from the SeaWiFS and MODIS sensors over coastal regions and open oceans. *Applied optics*, *49*(29), pp.5545-5560.

Anderson, S.M., Morton, J., and Mauersberger, K.. "Near-infrared absorption spectra of 16O3 and 18O3: Adiabatic energy of the 1A2 state?." The Journal of Chemical Physics 93.6 (1990): 3826-3832.

Draft

Anderson, Stuart M., Maeder, J., and Mauersberger, K. "Effect of isotopic substitution on the visible absorption spectrum of ozone." The Journal of chemical physics 94.10 (1991): 6351-6357

Bodhaine, B.A., Wood, N.B., Dutton, E.G. and Slusser, J.R., 1999. On Rayleigh optical depth calculations. *Journal of Atmospheric and Oceanic Technology*, *16*(11), pp.1854-1861.

Cox, C. and Munk, W., 1954. Measurement of the roughness of the sea surface from photographs of the sun's glitter. *Josa*, *44*(11), pp.838-850.

Frouin, R., Schwindling, M. and Deschamps, P.Y., 1996. Spectral reflectance of sea foam in the visible and near-infrared: In situ measurements and remote sensing implications. *Journal of Geophysical Research: Oceans*, *101*(C6), pp.14361-14371.

Koepke, P., 1984. Effective reflectance of oceanic whitecaps. *Applied optics*, *23*(11), pp.1816-1824.

Mobley, C.D., Werdell, J., Franz, B., Ahmad, Z. and Bailey, S., 2016. Atmospheric correction for satellite ocean color radiometry.

Morel, A. and Maritorena, S., 2001. Bio-optical properties of oceanic waters: A reappraisal. *Journal of Geophysical Research: Oceans*, *106*(C4), pp.7163-7180.

Rothman, L.S., Gordon, I.E., Babikov, Y., Barbe, A., Benner, D.C., Bernath, P.F., Birk, M., Bizzocchi, L., Boudon, V., Brown, L.R. and Campargue, A., 2013. The HITRAN2012 molecular spectroscopic database. *Journal of Quantitative Spectroscopy and Radiative Transfer*, *130*, pp.4-50.

Shettle, E.P. and Fenn, R.W., 1979. *Models for the aerosols of the lower atmosphere and the effects of humidity variations on their optical properties* (Vol. 79, No. 214). Air Force Geophysics Laboratory, Air Force Systems Command, United States Air Force.

Stramska, M. and Petelski, T., 2003. Observations of oceanic whitecaps in the north polar waters of the Atlantic. *Journal of Geophysical Research: Oceans*, *108*(C3).

Thuillier, G., Hersé, M., Foujols, T., Peetermans, W., Gillotay, D., Simon, P.C. and Mandel, H., 2003. The solar spectral irradiance from 200 to 2400 nm as measured by the SOLSPEC spectrometer from the ATLAS and EURECA missions. Solar Physics, 214(1), pp.1-22.

Wang, M., 2005. A refinement for the Rayleigh radiance computation with variation of the atmospheric pressure. *International Journal of Remote Sensing*, *26*(24), pp.5651-5663.

Werdell, P.J., Bailey, S.W., Franz, B.A., Morel, A. and McClain, C.R., 2007. On-orbit vicarious calibration of ocean color sensors using an ocean surface reflectance model. *Applied optics*, *46*(23), pp.5649-5666.